Time-resolved rheometry of drying liquids and suspensions

Pierre Lehéricey, Patrick Snabre, Audrey Delots, Niels Holten-Andersen, Thibaut Divoux

AUTHOR QUERY FORM

AIP Publishing	**Journal: J. Rheol.** **Article Number: JOR20-AR-00317**	**Please provide your responses and any corrections by annotating this PDF and uploading it to AIP's eProof website as detailed in the Welcome email.**

Dear Author,

Below are the queries associated with your article; please answer all of these queries before sending the proof back to AIP. Author please indicate the correct color processing option from the list below:

1. Author, please confirm Figure number(s) that should appear as color in print. Please know that a fee of $325 per figure will apply for figures printed in color.
2. Author, please confirm Figure number(s) that should appear as color online only, there will be no fees applied.
3. Author, your paper currently does not include any color figures for online or print. If color is needed please indicate which figures it should be applied to and whether it is color in print or online.

Article checklist: In order to ensure greater accuracy, please check the following and make all necessary corrections before returning your proof.

1. Is the title of your article accurate and spelled correctly?
2. Please check affiliations including spelling, completeness, and correct linking to authors.
3. Did you remember to include acknowledgment of funding, if required, and is it accurate?

Location in article	Query / Remark: click on the Q link to navigate to the appropriate spot in the proof. There, insert your comments as a PDF annotation.
Q1	Please check that the author names are in the proper order and spelled correctly. Also, please ensure that each author's given and surnames have been correctly identified (given names are highlighted in red and surnames appear in blue).
Q2	Please provide the keywords for this article.
Q3	Please confirm publisher name and location for Ref. 28, as we have inserted the required information.
Q4	Readers of print will only see figures in black and white. Please modify your text in the captions of Figs. 3–5, 7, 8, and 11 accordingly.
	Please check and confirm the Funder(s) and Grant Reference Number(s) provided with your submission: Please add any additional funding sources not stated above:

Thank you for your assistance.

Time-resolved rheometry of drying liquids and suspensions

Pierre Lehéricey,[1] Patrick Snabre,[2] Audrey Delots,[1] Niels Holten-Andersen,[1] and Thibaut Divoux[3,4,a)]

[1]*Department of Materials Science and Engineering, Massachusetts Institute of Technology, Cambridge, Massachusetts 02139*
[2]*Centre de Recherche Paul Pascal, CNRS UMR 5031, 33600 Pessac, France*
[3]*Univ Lyon, Ens de Lyon, Univ Claude Bernard, CNRS, Laboratoire de Physique, F-69342 Lyon, France*
[4]*MultiScale Material Science for Energy and Environment, UMI 3466, CNRS-MIT, 77 Massachusetts Avenue, Cambridge, Massachusetts 02139*

(Received 22 December 2020; final revision received 13 March 2021; published xx xx 2021)

Abstract

From paints to food products, solvent evaporation is ubiquitous and critically impacts product rheological properties. It affects Newtonian fluids by concentrating any nonvolatile components and viscoelastic materials, which harden up. In both of these cases, solvent evaporation leads to a change in the volume of the sample, which makes any rheological measurements particularly challenging with traditional shear geometries. Here, we show that the rheological properties of a sample experiencing "slow" evaporation can be monitored in a time-resolved fashion by using a zero normal force controlled protocol in a parallel-plate geometry. Solvent evaporation from the sample leads to a decrease of the normal force, which is compensated at all times by a decrease of the gap height between the plates. As a result, the sample maintains a constant contact area with the plates, despite the significant decrease of its volume. We validate the method under both oscillatory and continuous shear by accurately monitoring the viscosity of water–glycerol mixtures experiencing evaporation and a relative volume decrease as large as 70%. Moreover, we apply this protocol to drying suspensions. Specifically, we monitor a dispersion of charged silica nanoparticles undergoing a glass transition induced by evaporation. While the decrease in gap height provides a direct estimate of the increasing particle volume fraction, oscillatory and continuous shear measurements allow us to monitor the evolving viscoelastic properties of the suspension in real time. Overall, our study shows that a zero normal force protocol provides a simple approach to bulk and time-resolved rheological characterization for systems experiencing slow volume variations. © *2021 The Society of Rheology.* https://doi.org/10.1122/8.0000214

I. INTRODUCTION

Evaporation of volatile liquids alters the rheological properties of numerous materials from Newtonian liquids (e.g., water in water–glycerol mixtures) to viscoelastic liquids and soft solids (e.g., volatile solvents in suspensions and gels) [1,2]. On the one hand, evaporation can be an issue that needs to be limited, for instance, when performing rheological measurements to characterize functional properties of samples with volatile solvents such as paints or inks, etc. [3]. In that case, rheological experiments are performed with a solvent trap, or an oil rim at the sample periphery for parallel-plate and cone-and-plate geometry, or even in an insulated chamber [4–6]. On the other hand, evaporation can be used to alter the microstructure of a sample and tune its properties, often through a solgel or sol–glass transition. For instance, solvent evaporation plays a key role in the formation of films with self-assembled nanostructure [7,8]. Moreover, solvent evaporation can be used to concentrate a suspension of particles into a solid, whose microstructure and mechanical properties can be accurately controlled [9–12]. Similarly, a solvent can also be evaporated from a polymer mixture to create a hardened composite. Contrary to UV-curing where the addition of a photoinitiator is needed to form an interconnected network from low molecular weight components through photopolymerization [13], solvent evaporation can happen with or without curing agents. This is the case of coatings where the formation of intermolecular or interparticle bonds starts after evaporation [14,15]. Finally, natural materials such as skin, hair, and horns are classical examples of extraorganismal biomacromolecular materials that undergo various levels of dehydration in time and space as part of their life cycle [16]. In fact, material dehydration has been documented as an effective biological material design strategy for achieving unique mechanical properties, as in some cases, the synergistic effect of dehydration and local macromolecular network densification can lead to exceptional mechanical strength. This is the case of the beak of the Humboldt squid, which shows a strong gradient in water content, and whose tip is among the hardest and stiffest wholly organic materials known [17].

A key challenge in studies of complex fluids or soft solids with volatile solvents remains how to quantify the changes induced by solvent evaporation on the rheological properties of a system experiencing dehydration. Evaporation is a nonisochoric process, which often involves spatially heterogeneous dynamics that leads to concentration gradients [18]. As a result, time-resolved rheological measurements at the macroscale are very challenging [19]. This is the reason why most of the experimental effort has been focused on indirect measurements, e.g., based on film surface topography [20],

a)Author to whom correspondence should be addressed; electronic mail: Thibaut.Divoux@ens-lyon.fr

and local investigation techniques such as active and passive microrheology [21–24].

Here, we propose to perform time-resolved measurements of the macroscopic rheological properties of samples experiencing slow evaporation, i.e., slow enough to safely assume that the sample does not develop any solid plug stopping dehydration. Specifically, after placing the sample in a parallel-plate geometry connected to a stress-controlled rheometer, we use a zero normal force (ZNF) protocol, in which the normal force exerted on the sample is maintained equal to zero, while the gap height is free to adjust and compensate for the decrease of the sample volume. This method, which was previously shown to be efficient in measuring rheological properties during nonisochoric gelation of agarose dispersions [25,26] and organogels [27], is employed here to monitor the rheological properties of drying Newtonian fluids and charged colloidal suspensions, as first suggested in [28]. We show that the ZNF protocol allows us to monitor the continuous increase in viscosity of a dehydrating water–glycerol mixture, as well as the discontinuous changes in viscoelastic properties of a drying colloidal suspension during its glass transition. This study thereby paves the way for systematic time-resolved rheological measurements on macroscopic samples of complex fluids experiencing strong nonisochoric transitions induced by solvent evaporation.

The article is organized as follows: in Sec. II, we describe the samples characterized in the drying experiments and motivate the ZNF protocol. In Sec. III, we validate this protocol by confirming the invariant viscosity of a drying water sample monitored over several hours. We then apply the ZNF protocol to monitor the increasing viscosity of drying water–glycerol mixtures as water progressively evaporates. Drying experiments performed either under oscillatory or continuous shear demonstrate that the ZNF protocol allows us to monitor sample viscosity with high precision, while the sample volume decreases by up to 70%. Finally, we apply the ZNF protocol to monitor the drying of a stable colloidal suspension. Here, we further validate the ZNF protocol by confirming that the estimate of the critical volume fraction associated with the dehydration-induced glass transition is in good agreement with values from the literature. Moreover, interpretations based on image correlation analysis from simultaneous images recorded during rheological measurements on the colloidal suspensions suggest that data collected under continuous shear, rather than oscillatory shear, provide more accurate information on dehydration-induced microstructural changes, likely due to suppressed concentration gradients.

II. MATERIAL AND METHODS

A. Rheological setup

Rheological measurements are performed with a parallel-plate geometry (diameter $2R = 25$ mm), connected to a stress-controlled rheometer (MCR 302, Anton Paar). The bottom plate consists of a Peltier module (P-PTD 200), which sets the temperature of the sample. All the experiments were performed at $T = 25\,^{\circ}$C. The upper plate is smooth and made of stainless steel (PP 25). Samples are loaded with a micropipette, which allows us to precisely fill the cell, whose initial gap is set by default to $h_0 = 500\,\mu$m. The normal force is reset to $F_N = 0$ N immediately after loading the sample and prior to the start of the experiment, which simply consists of initiating the dehydration of the sample at constant temperature. The parallel-plate geometry is topped by a Peltier temperature-controlled hood (H-PTD 200), which consists of a cylinder (diameter $2R^* = 95$ mm) centered with the rotation axis of the upper plate (Fig. 1). Besides temperature control, the hood strongly reduces convection around the sample and allows us to control the evaporation rate by controlling the spacing between the foot of the hood and the bottom plate (the hood is typically placed at about 1 mm above the bottom plate). It takes about 30 min for the humidity ratio (HR) to reach saturation under the hood for an experiment started at ambient HR = 42% [see Fig. 8(b) in Appendix A, which shows that a steady state is reached beyond 30 min].

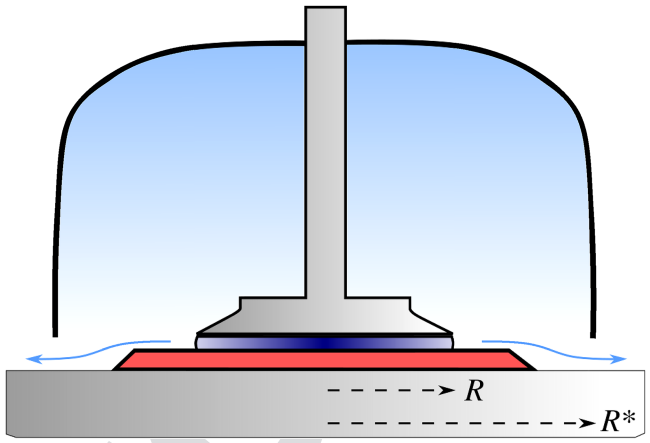

FIG. 1. Schematic view of the experimental setup. The sample is placed in a parallel-pate geometry (diameter $2R = 25$ mm), whose bottom plate contains a Peltier element setting the temperature. The upper plate is connected to a stress-controlled rheometer. A cylindrical hood (diameter $2R^* = 95$ mm) ensures a sample environment with control over the temperature and the evaporation (blue arrows) by setting the distance between the bottom plate and the hood such that the humidity under the hood is close to saturation.

Finally, in some experiments, the bottom plate and the Peltier module are replaced by a transparent glass plate to visualize the sample. In that case, images of the sample are taken through the transparent plate, which sits atop the support containing a semireflective blade forming a 45° angle with respect to the rotation axis of the rotor.

Images are taken with a camera (Canon EF 100 mm, aperture = 2.8 mounted on a DSLR Canon 6D), which is focused on the semireflective blade. In this configuration, the entire surface of the plate is imaged with a spatial resolution of 352 μm/pixel.

B. Samples

In the present study, we monitor the drying of three different samples: (i) distilled water, (ii) water–glycerol mixtures with an initial weight fraction in glycerol (Sigma Aldrich, G9012, $\geq 99.5\%$) ranging between 20 and 60 wt. %, and (iii) a suspension of silica nanoparticles (Ludox HS-40, Sigma Aldrich) with a particle diameter of 12 nm and a specific

surface area of $220\,\mathrm{m^2\,g^{-1}}$. The mass fraction of the as-purchased-dispersion is 40 wt. %, which corresponds to an initial volume fraction of $\phi_0 = 0.23$. The suspension was degassed for 10 h under vacuum before testing. The colloids are stabilized by the presence of negative silanol groups at their free surface, which attract Na^+ cations in the solution, hence forming an electrical double layer (EDL) responsible for the strong repulsive interaction between colloids. Several studies have shown that these colloids and their EDL display an elastic behavior well below the usual random close packing fraction. For Ludox HS-40, the critical volume fraction beyond which a solidlike response dominates is $\phi_c^{(\mathrm{ref})} = 0.32$ [29–32].

C. Constant gap vs zero normal force protocol

Following the loading of the sample, the top plate is put in contact with the sample, and the normal force is reset to $F_N = 0\,\mathrm{N}$. As the volatile components of the sample slowly evaporates at the periphery of the plate, the volume of the sample decreases (Fig. 2). On the one hand, if the gap height h_0 is maintained constant, the evaporation leads to a decrease of the curvature radius of the fluid meniscus at the periphery of the cell. As a result, capillary forces pull on the upper plate of the geometry, leading to an increase of the absolute value of the normal force, which is about $|\Delta F_N| = \gamma \cdot 2\pi R$, where γ is the surface tension at the air–fluid interface, and $2R$ is the plate's diameter. In case the sample considered is water, $|\Delta F_N| \simeq 6\,\mathrm{mN}$, which is an order of magnitude larger than the sensitivity of the rheometer's normal force sensor (0.5 mN). Eventually, as the evaporation goes on, the contact line of the sample at the plate periphery contracts radially and the amount of the sample left inside the geometry does not cover the entire surface of the plates, yielding a systematic error in the determination of the shear stress. On the other hand, if the normal force is maintained constant, equal to zero, while the gap height is left free to vary, the latter will decrease to compensate for the increase in the capillary forces induced by the sample evaporation and indeed maintain $F_N = 0\,\mathrm{N}$. As a result, the sample will occupy a constant surface area identical to that of the plates, thus allowing for bulk rheological measurements, while the sample is slowly evaporating. In the rest of the paper, we validate and use this ZNF protocol to monitor the temporal evolution of the rheological properties of drying Newtonian fluids and viscoelastic samples.

III. RESULTS AND DISCUSSION

A. Measuring the viscosity of a drying Newtonian liquid

To validate the ZNF protocol, we monitor the viscosity of a single-component Newtonian fluid sample composed of distilled water during evaporation from the parallel-plate geometry at $T = 25\,^\circ\mathrm{C}$ over 30 min. The experiment is repeated twice in two different configurations. In the first experiment, the sample dynamics viscosity $\eta' = G''/\omega_0$, where G'' is the viscous modulus, is assessed by oscillations of constant strain amplitude $\gamma_0 = 50\%$ at a frequency $f_0 = \omega_0/(2\pi) = 0.2\,\mathrm{Hz}$. In the second experiment, we determine the *shear viscosity* $\eta = \sigma/\dot{\gamma}$, where σ is the measured shear stress monitored under continuous shear at a fixed shear rate $\dot{\gamma} = 10\,\mathrm{s^{-1}}$. The results are summarized in Fig. 3.

In both cases, the normal force is successfully maintained equal to zero (within 2%) [Figs. 3(a) and 3(d)], while the gap height decreases by about 4% over the entire duration of the experiment to compensate for the decrease in the sample volume induced by evaporation [Figs. 3(b) and 3(e)]. Moreover, the viscosity is measured to be constant throughout both types of experiments, i.e., the *dynamic viscosity* η' determined under oscillations, and the *shear viscosity* η are both constant in time and within error bars compatible with tabulated viscosity values of water at 25 °C ($\eta = 0.89\,\mathrm{mPa\,s}$—see, for instance, IAPWS 2008) [Figs. 3(c) and 3(f)]. Note that the viscosity measurements under oscillatory shear [Fig. 3(c)] show more noise than under continuous shear [Fig. 3(f)]. This observation can be explained by the fact that the torque applied during an oscillatory shear experiment (2 nN m) is closer to the lower torque detection limit (∼0.5 nN m) than the torque applied during a steady-shear experiment (420 nN m).

Following the same ZNF protocol, we were able to monitor the viscosity of water under continuous shear for more than 10 h during which the gap decreases by about 60% (see Fig. 8 in Appendix A). The continuous relative gap

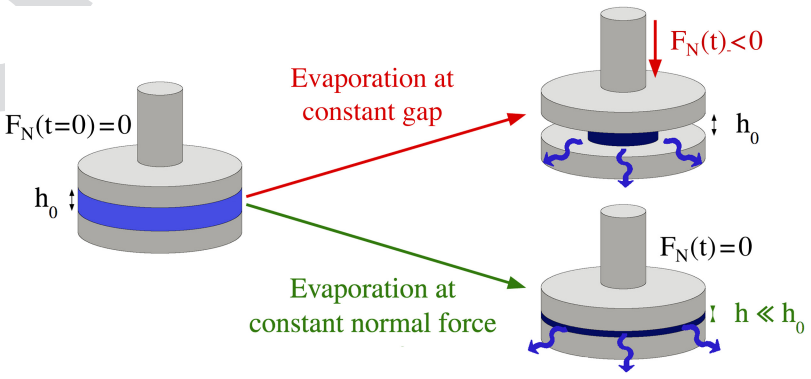

FIG. 2. Schematics of the comparison between drying experiments conducted at constant gap and constant normal force, respectively. At constant gap, evaporation leads to a decrease in the contact area between the sample and the plates. At constant normal force, to maintain a zero normal force on the upper plate, the gap decrease compensates for the sample evaporation such that the apparent contact area between the plates and the sample remains the same.

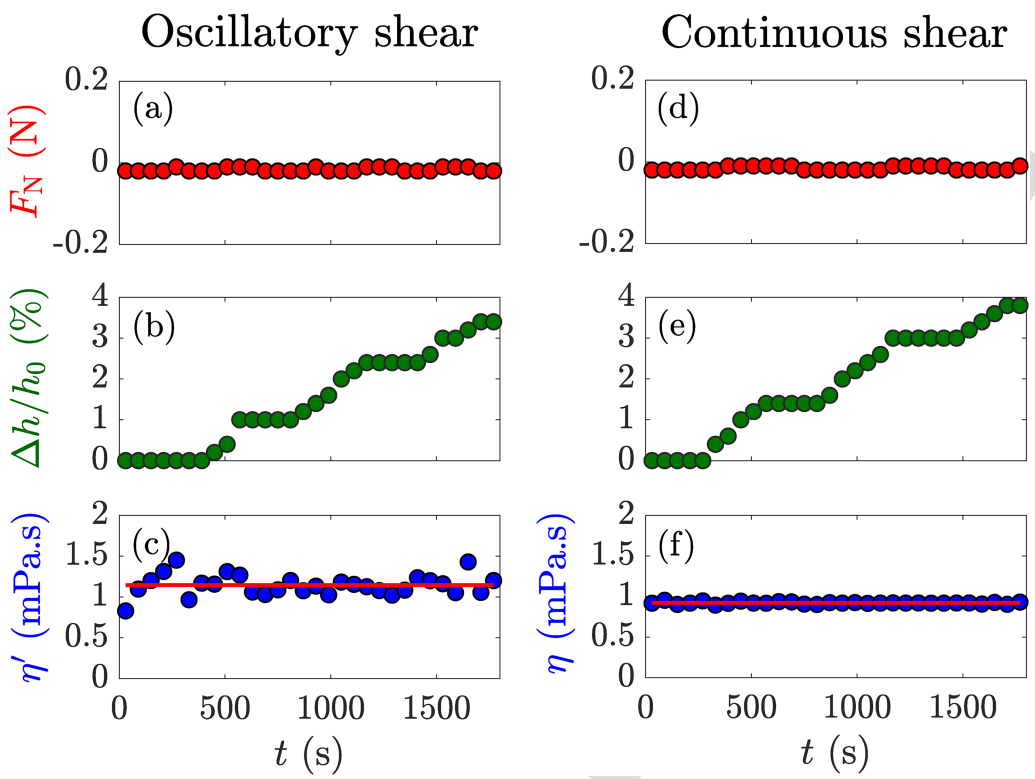

FIG. 3. Viscosity measurement with the zero normal force protocol under (a)–(c) oscillatory shear and (d)–(f) continuous shear on a drying water sample. In both cases, we report the temporal evolution of (a) and (d) the applied normal force F_N, (b) and (e) the relative gap decrease $\Delta h/h_0$, (c) the dynamic viscosity $\eta' = G''/\omega_0$, and (f) the shear viscosity $\eta = \sigma/\dot{\gamma}$. Experiments performed at 25 °C, with $h_0 = 500\,\mu$m. Oscillatory measurements reported in (a)–(c) are performed at a frequency $f_0 = \omega_0/(2\pi) = 0.2$ Hz with a constant strain amplitude $\gamma_0 = 50\%$. Continuous shear measurements reported in (d)–(f) are performed at $\dot{\gamma} = 10\,s^{-1}$. In (c) and (f), the red line corresponds to the mean value of the viscosity computed over the duration of the experiment, i.e., $\eta' = (1.14 \pm 0.12)$ mPa s and $\eta = (0.92 \pm 0.01)$ mPa s, respectively.

Q4

decrease $\Delta h/h_0$ over time is a direct measurement of the evaporation rate, which allows us to compute the mass flux of water J_m leaving the shear cell as $J_m \simeq 0.3\,g\,m^{-2}\,s^{-1}$ at 25 °C. This estimate is in good agreement with the values reported in the literature measured with different experimental techniques [33,34]. Repeating the drying experiment under continuous shear at different temperatures allows us to confirm that the temperature dependence of the evaporation rate follows a scaling that is in agreement with previous work [35] (see Fig. 9 in Appendix B). Furthermore, the viscosity was found to decrease with increasing temperature likewise in agreement with reported values of water viscosity [36]. In conclusion, the results from this section on single-component Newtonian fluids demonstrate the validity of the ZNF protocol.

B. Measuring the viscosity of drying water–glycerol mixtures

In this section, we monitor the viscosity of a Newtonian fluid composed of two miscible liquids, only one of which is volatile. Specifically, we apply the ZNF protocol to the study of drying water–glycerol mixtures by measuring the increase in viscosity as a function of water evaporation. Similar to Sec. III A, we monitor the drying of the samples by applying either an oscillatory shear (γ_0 =50%, $f_0 = 0.3$ Hz) or a continuous shear ($\dot{\gamma} = 10\,s^{-1}$), thereby providing measurements of the dynamic viscosity η' and the shear viscosity η, respectively.

We first discuss results from a mixture with a 20 wt. % glycerol content, which are reported in Fig. 4. A constant normal force is maintained during 4 h of both oscillatory and continuous shear [Figs. 4(a) and 4(e)]. The gap thickness decreases by about 70 wt. % in both experiments due to water evaporation [Figs. 4(b) and 4(f)], whereby the weight fraction in glycerol increases as manifested by an increase in sample viscosity [Figs. 4(c) and 4(g)]. Moreover, the relative gap decrease follows an exponential behavior with a characteristic time $\tau \simeq 4.0$ h and 3.1 h for continuous and oscillatory shear tests, respectively. Such slow down of the evaporation in both types of experiment are due to a change in the water activity. Indeed, the drying kinetics of the sample is inversely proportional to the difference $(a - a_e)$ between the activity a of water in the water–glycerol mixture and the relative humidity $a_e \simeq 0.42$ at the edge of the hood [37]. As water evaporates, the activity decreases [38] from $a \simeq 0.95$ for an initial glycerol content of 20% to $a \simeq 0.56$ for a glycerol content of 50%. Evaporation increases the glycerol volume fraction in the sample, which, in turn, continuously reduces the water activity a and thereby the evaporation rate.

Let us now have a closer look at the evolution of the sample dynamic viscosity η' reported in Fig. 4(c). In the first stage of the drying experiment, i.e., for $t < t^* = 1.2$ h, the

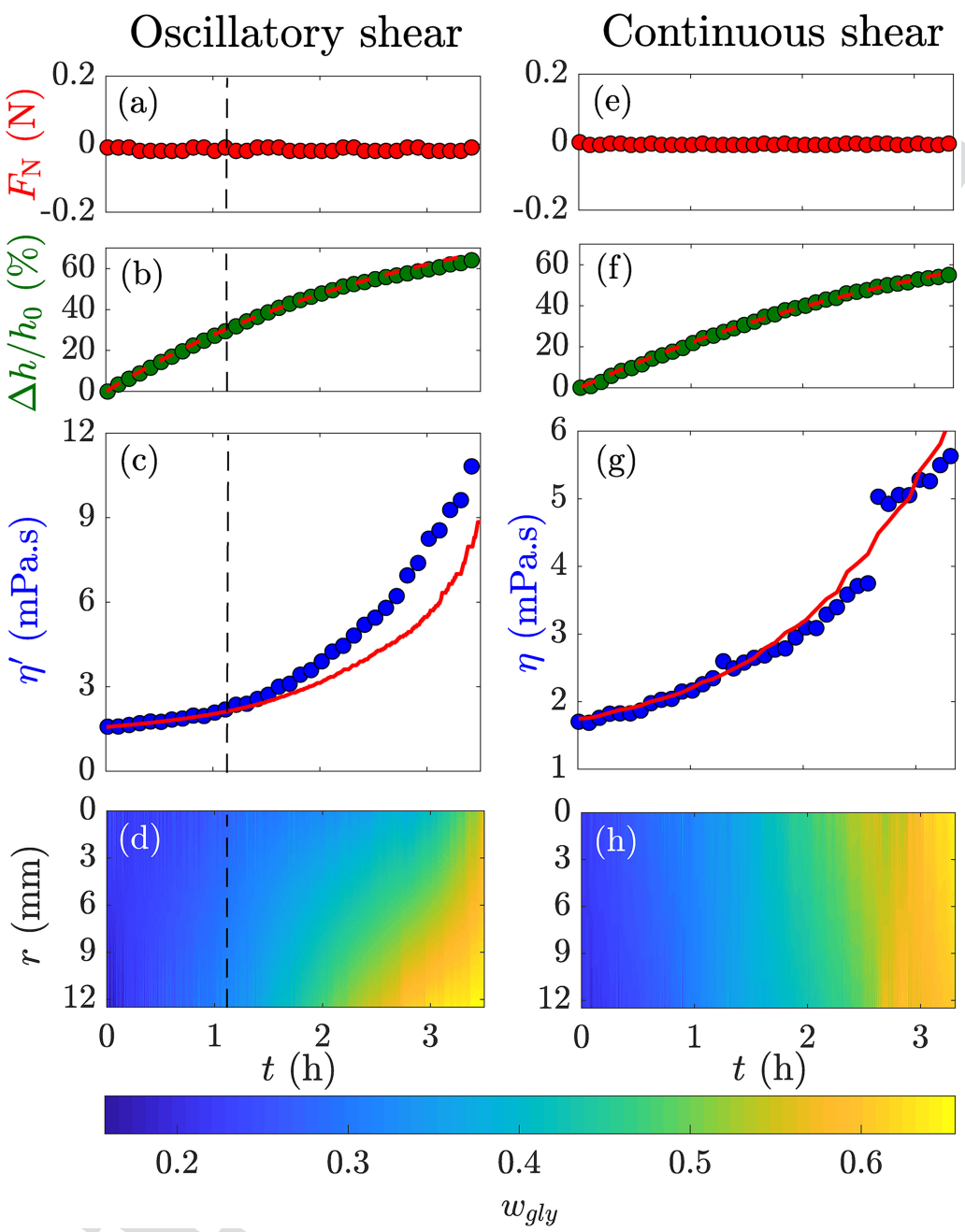

FIG. 4. Drying experiments on a water–glycerol mixture with the initial glycerol content of 20 wt. % during which the sample's rheological properties are measured with the ZNF protocol under (a)–(d) oscillatory shear [frequency $f_0 = \omega_0/(2\pi) = 0.3$ Hz and constant strain amplitude $\gamma_0 = 50\%$] and (e)–(h) continuous shear ($\dot{\gamma} = 10\,\mathrm{s}^{-1}$). In both cases, we report the temporal evolution of (a) and (e) the applied normal force F_N, (b) and (f) the relative gap decrease $\Delta h/h_0$, (c) the dynamic viscosity $\eta' = G''/\omega_0$, and (g) the shear viscosity $\eta = \sigma/\dot{\gamma}$, and (d) and (h) a spatiotemporal diagram of an estimated concentration gradient in the sample along the radial direction. Experiments are performed at $T = 25\,^\circ$C. In (b) and (f), the dashed red curve corresponds to an exponential fit of the relative gap decrease with a characteristic time of 3.1 and 4 h, respectively. In (c) and (g), the continuous red curve corresponds to the tabulated values [36] of the shear viscosity of water–glycerol mixtures at $T = 25\,^\circ$C, assuming that the glycerol concentration, inferred from the gap decrease, remains homogeneous. The vertical dashed line in (a)–(d) corresponds to the time $t = t^*$ beyond which the glycerol concentration is no longer homogeneous along the radial direction.

dynamic viscosity of the water–glycerol mixture agrees well with tabulated viscosity values of water–glycerol mixtures [36] [continuous red line in Fig. 4(c)], based on glycerol concentrations determined from the gap decrease [Fig. 4(b)]. This result suggests that the glycerol concentration is homogeneous in the shear cell. However, for $t > t^*$, the dynamic viscosity significantly differs from the tabulated values. This discrepancy most likely originates from the formation of a concentration gradient along the radial direction of the shear cell. Indeed, concentration gradients were reported in drying experiments performed in geometries of fixed volume [37] for Peclet numbers, $Pe = R^2/(D\tau) > 1$, where R is the sample size (here the plate radius), D is the diffusion coefficient of glycerol in water, and τ is the characteristic time of

evaporation. In that context, $D\tau$ represents the square of the diffusive length-scale in the sample of size R. For the experiments reported in Fig. 4(c), $Pe \simeq 40 > 1$ (with $\tau \simeq 3$ h and $D = 3.5 \times 10^{-10}$ m^2 s^{-1} for a 20% mass fraction in glycerol [39]), which supports the idea that the glycerol concentrates at the rim of the parallel-plate geometry, forming a ring of nonvolatile fluid, which limits the water evaporation. In contrast, the viscosity measured under continuous shear is in excellent agreement at all times with literature values [36], which suggests that the glycerol concentration remains more homogeneous along the radial direction under continuous shear flow conditions.

To make sense of the time-evolution of the dynamic viscosity for $t > t^*$ [Fig. 4(c)], we assume the existence of a linear gradient of glycerol along the radial direction with a larger glycerol concentration at the edge of the plate. The glycerol concentration at position r and time t reads: $w_{\rm gly}(r, t) = w_{\rm gly}(0, t) + \alpha(t)r$, where $w_{\rm gly}(0, t)$ is the mass fraction at the center of the geometry ($r = 0$) and $\alpha(t)$ the concentration gradient. We can determine the values of $w_{\rm gly}(0, t)$ and $\alpha(t)$ at each point in time, using mass conservation and the viscosity measured with the rheometer during the drying experiment. First, the mass conservation in glycerol reads $\bar{w}_{\rm gly}(t)h(t) = w_{\rm gly}(0, t = 0)h(0)$, where h denotes the gap height, $\bar{w}_{\rm gly}(t)$ stands for the average mass fraction of glycerol at a time t, and $w_{\rm gly}(0, t = 0)$ is the initial volume fraction in glycerol, originally homogeneous in the sample. The average mass fraction provides a first equation to determine $w_{\rm gly}(0, t)$ and $\alpha(t)$, namely,

$$\bar{w}_{\rm gly}(t) = \frac{1}{R}\int_0^R w_{\rm gly}(r, t)\mathrm{d}r = w_{\rm gly}(0, t) + \alpha(t)\frac{R}{2}. \quad (1)$$

Second, the rheometer software gives us the viscosity of the sample computed at the rim of the geometry, without any single-point correction [40]. Using tabulated values of the viscosity for water–glycerol mixtures [36], we compute the mass fraction of glycerol at the edge of the shear cell,

$$w_{\rm gly}(r = R, t) = w_{\rm gly}(0, t) + \alpha(t)R. \quad (2)$$

Finally, the resolution of the linear system of Eqs. (1) and (2) leads to the determination of the glycerol concentration at the center of the cell $w_{\rm gly}(0, t)$ and the gradient $\alpha(t)$ at all time during the experiment.

The profile of glycerol concentration obtained with this method is shown as a spatiotemporal diagram in Fig. 4(d). The same approach applied to the viscosity measurement performed under continuous shear are also reported in Fig. 4(h). We note that a gradient assumed here as linear develops beyond t^* for oscillatory measurements, with $\alpha(t) > 0$, whereas the gradient remains negligible $\alpha(t) \simeq 0$ for measurement under continuous shear at $\dot{\gamma} = 10\,\mathrm{s}^{-1}$ (see Fig. 10 in Appendix C). Continuous shear allows for the homogenization of the water–glycerol mixture while the water evaporates, whereas oscillatory shear is less efficient in doing so. Strikingly, this result for continuous shear depends on the shear intensity $\dot{\gamma}$, and imposing a larger shear rate leads to a detrimental effect, e.g., imposing $\dot{\gamma} = 100\,\mathrm{s}^{-1}$ leads to the formation of a gradient, with $\alpha(t) < 0$ (see Fig. 11 in Appendix D). In that case, the volume fraction of glycerol is larger at the center of the shear cell as due to the influence of $\dot{\gamma}$ on the diffusion of glycerol in water [41]. Therefore, we conclude that a continuous shear of moderate intensity is the most appropriate method to monitor the time-evolution of the viscosity of the dehydrating water–glycerol mixture.

To illustrate the robustness of our results, we have repeated the drying experiments for water–glycerol mixtures with two other glycerol mass fractions, namely, 40 and 60 wt. %. The viscosity of the drying mixtures is monitored as before, with the ZNF protocol under oscillatory and continuous shear. We report the viscosity as a function of the glycerol concentration for the three water–glycerol mixtures (i.e., 20, 40, and 60 wt. %) in Fig. 5(a), which displays the mixture viscosity as a function of the glycerol weight fraction determined from the gap decrease, assuming that only water is evaporating. The datasets for the three mixtures are reported separately in Figs. 5(b)–5(d). Except for the long-time measurements in the case of the 20 wt. % discussed above, all the experimental data are in excellent agreement with tabulated viscosity values of water–glycerol mixtures of various composition, in the absence of any evaporation. These results suggest that the 40 and 60 wt. % glycerol solutions are much less prone to develop concentration gradients. Our results, therefore, demonstrate that the ZNF protocol allows us to accurately monitor the continuously increasing viscosity of a drying Newtonian liquid.

C. Monitoring the drying-induced glass transition in a colloidal suspension

In this section, we use the ZNF protocol to monitor the rheological properties of a drying aqueous suspension of charged silica nanoparticles. The experiments are here performed in a parallel-plate geometry, whose bottom plate is transparent in order to visualize the sample (see Sec. II A for details).

We first discuss the case of a drying aqueous suspension monitored by oscillatory shear. The linear viscoelastic moduli are determined at $f_0 = 1$ Hz, with a variable strain amplitude γ_0, which is adjusted to the sample viscoelastic properties so as to optimize the sensitivity of the measurement, without affecting the gelation process [3]. We found empirically that a good compromise consists in imposing a large strain amplitude $\gamma_0 = 50\%$, while the sample is mainly viscous before switching to a small amplitude $\gamma_0 = 0.01\%$ as soon as G' becomes comparable to G'' to avoid damaging the soft solid that is forming as a result of the solvent evaporation. Such a strain-adapted protocol allows us to monitor the temporal evolution of the elastic and viscous modulus of the suspension over 12 h, while the solvent evaporates. The results are plotted as a function of time in Fig. 6(d), and the same data are reported in Fig. 7(a) as a function of the volume fraction, which is inferred from the gap variation.

At the start of the experiment, the sample is liquid and characterized solely by its viscous modulus G'', which

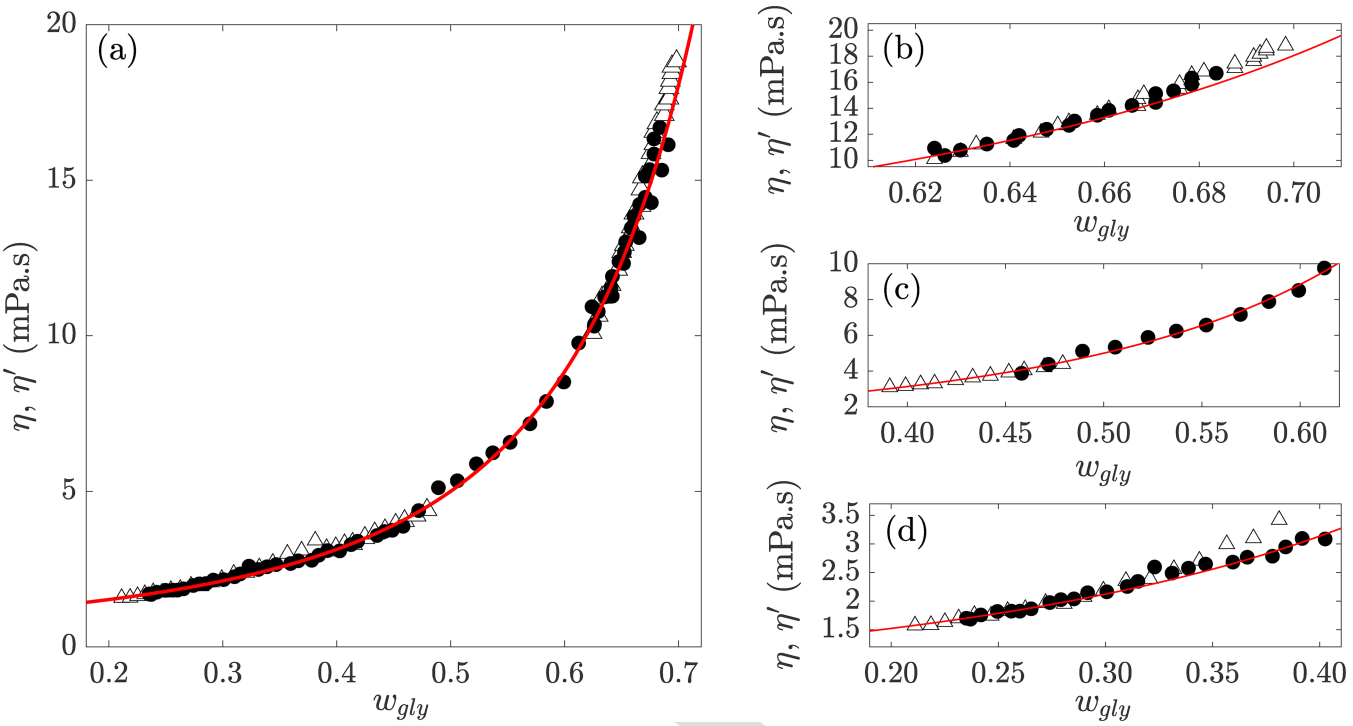

FIG. 5. Drying experiments on three different water–glycerol mixtures (initial mass fractions in glycerol of 20, 40, and 60 wt. %) during which the viscoelastic moduli and the shear viscosity are measured with the ZNF protocol under oscillatory shear and continuous shear, respectively. (a) Dynamic viscosity $\eta' = G''/\omega_0$ (△) and shear viscosity $\eta = \sigma/\dot{\gamma}$ (•). (b)–(d) Focus on individual experiments with an initial mass fraction of about (b) 60, (c) 40, and (d) 20 wt. %. Experiments are performed at $T = 25\,^{\circ}\mathrm{C}$. Oscillatory measurements are performed at $f_0 = 0.3$ Hz and $\gamma_0 = 50\%$, $f_0 = 0.5$ Hz and $\gamma_0 = 40\%$, and $f_0 = 0.3$ Hz and $\gamma_0 = 30\%$ for an initial mass fraction of glycerol of 20, 40, and 60 wt. %, respectively. Continuous shear experiments are performed at $\dot{\gamma} = 10\,\mathrm{s}^{-1}$. The red curve corresponds to the tabulated values of the shear viscosity of water–glycerol mixtures measured at $T = 25\,^{\circ}\mathrm{C}$ on series of homogeneous samples of fixed concentrations, in the absence of any evaporation [36].

slowly increases as the solvent evaporates [Fig. 6(d)]. At $t \simeq 1.5$ h, the sample shows a linear viscoelastic response such that $G' < G''$. Beyond $t \simeq 1.5$ h, both modulus increase as a result of the solvent evaporation up to $t \simeq 4.5$ h at which G' crosses G'', marking the emergence of a yield stress. The crossing of G' and G'' marked by a dashed vertical line in Figs. 6(d) and 7(a) occurs at a volume fraction $\phi_c \simeq 0.35$, which is in reasonable agreement with the value expected for Ludox HS-40, i.e., $\phi_c^{(\mathrm{ref})} \simeq 0.32$ [29–32]. Note that up to ϕ_c, the normal force is correctly maintained within the interval $F_N = (0.00 \pm 0.01)$ N [Fig. 6(a)], while the relative gap decrease speeds up before reaching ϕ_c [Fig. 6(b)]. Beyond the intersection of G' and G'', i.e., for $t > 4.5$ h (or $\phi > 0.35$), both G' and G'' increase up to $t \simeq 6$ h, where they reach a plateau such that $G' > G''$. Interestingly, the viscoelastic plateau coincides with the cessation of the gap decrease, which suggests that the evaporation has completely stopped beyond $t = 6$ h. Finally, for $t > 9$ h, both G' and G'' decrease while the gap stays constant, which hints at some local reorganization of the colloidal glass, without any supplemental loss of solvent.

To confirm this scenario, we take advantage of the transparent bottom plate of the shear cell in which the drying experiment is conducted (see Sec. II A). Images of the entire surface of the sample shot through the transparent bottom plate and taken every 3 or 10 min in continuous or oscillatory shear experiments, respectively, allow us to quantify the local dynamics associated with the evaporation. The degree of correlation between two images separated by a lag-time τ is determined by the ensemble-average intensity correlation function $g_2(t, \tau)$ defined as follows:

$$g_2(t, \tau) = \frac{\langle I_p(t).I_p(t+\tau)\rangle_p}{\langle I_p(t)\rangle_p.\langle I_p(t+\tau)\rangle_p}, \qquad (3)$$

where I_p represents the brightness of the pixel p and $\langle\cdots\rangle_p$ the average over all the pixels [42,43]. The correlation function is further normalized into a function noted $g_2^*(t, \tau)$, which satisfies $g_2^*(t, \tau = 0) = 1$. The normalized correlation function is computed at a frame rate of about 1.6 mHz in oscillatory shear and 5 mHz in continuous shear, with a lag time τ ranging between 0 and 1 h. The results are pictured in a lag-time temporal diagram in Fig. 6(c). At any point in time for $t < 6$ h, the images slowly decorrelate over $\tau = 1$ h. The rate of decorrelation decreases abruptly in the vicinity of the gelation point ($t_c = 4.5$ h) before stopping completely at $t = 6$ h when the elastic and viscous moduli reach a plateau. The lack of decorrelation beyond 6 h confirms that the cessation of the gap decrease visible in Fig. 6(b) marks the end of the evaporation, which results from the formation of a solid crust at the sample edge. Such a solid crust isolating the sample from the ambient atmosphere is indeed visible, when separating the two plates at the end of an experiment.

We now turn to drying experiments performed on the suspension of silica particles under continuous shear, at

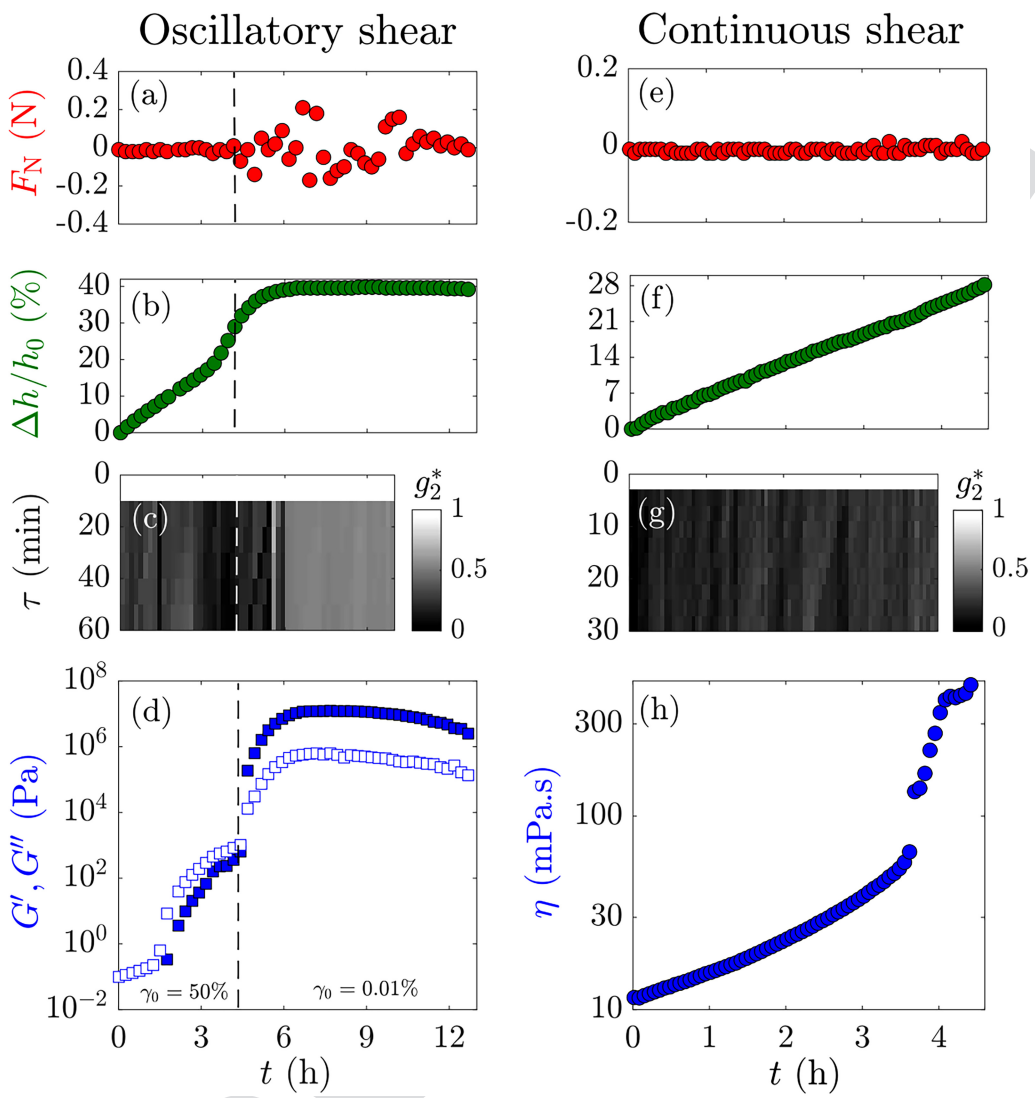

FIG. 6. Drying experiments on a suspension of silica nanoparticles of initial volume fraction $\phi_0 = 0.23$ during which the viscoelastic moduli and the viscosity are measured with the ZNF protocol under (a)–(d) oscillatory shear [frequency $f_0 = 1$ Hz, and strain amplitude $\gamma_0 = 50\%$ up to $t = 4.5$ h, and $\gamma_0 = 0.01\%$ for $t > 4.5$ h] and (e)–(h) continuous shear ($\dot{\gamma} = 10\,\mathrm{s}^{-1}$), respectively. In both cases, we report the temporal evolution of (a) and (e) the applied normal force F_N, (b) and (f) the relative gap decrease $\Delta h/h_0$, (c) and (g) lag-time temporal diagrams computed from the correlation of sample images taken through the transparent bottom plate, (d) the elastic and viscous moduli G' (■) and G'' (□), and (h) the shear viscosity $\eta = \sigma/\dot{\gamma}$. The vertical dashed line in (d) marks the crossing of G' and G'' at $t = t_c$. Experiments performed at constant temperature ($T \simeq 21°$C) in a parallel-plate geometry.

$\dot{\gamma} = 10\,\mathrm{s}^{-1}$. The results, including the shear viscosity, are reported as a function of time in Figs. 6(e)–6(h) and of the volume fraction in Fig. 7(b). As the solvent evaporates, the viscosity rises over time at increasing speed, before reaching a plateau at $t \simeq 4$ h, which can be attributed to the presence of spatial heterogeneities in a sample increasingly glassy [Fig. 6(h)]. The normal force is correctly set to $F_N = (0.00 \pm 0.01)$ N [Fig. 6(e)], while the relative gap decrease shows a somewhat linear trend over the 4.5 h that the experiment lasts [Fig. 6(f)]. Note that the total relative gap decrease is $\Delta h/h_0 \simeq 28\%$ at $t = 4.5$ h, which is comparable to the value reached at the same time for experiments performed under oscillatory shear [see Fig. 6(b)]. However, here the gap decrease accompanies a spatially homogeneous increase of the particle volume fraction, as confirmed by images of the drying suspension. Indeed, the normalized correlation function $g_2^*(t, \tau)$ pictured in Fig. 6(g) shows roughly the same rate of decorrelation as a function of the lag-time τ for the entire duration of the experiment. This observation shows that, in stark contrast to the experiments performed under oscillatory shear, drying experiments performed under constant shear yield a spatially more homogeneous sample, thus preventing the formation of a solid crust.

As supplemental evidence that the drying colloidal suspension remains homogeneous under continuous shear, we find that the corresponding viscosity measured as a function of time, and reported in Fig. 7(b) as a function of the volume fraction ϕ, is well-described by the Quemada model that reads [44]

$$\eta = \eta_s \left(1 - \frac{\phi}{\phi_{\max}}\right)^{-2}, \tag{4}$$

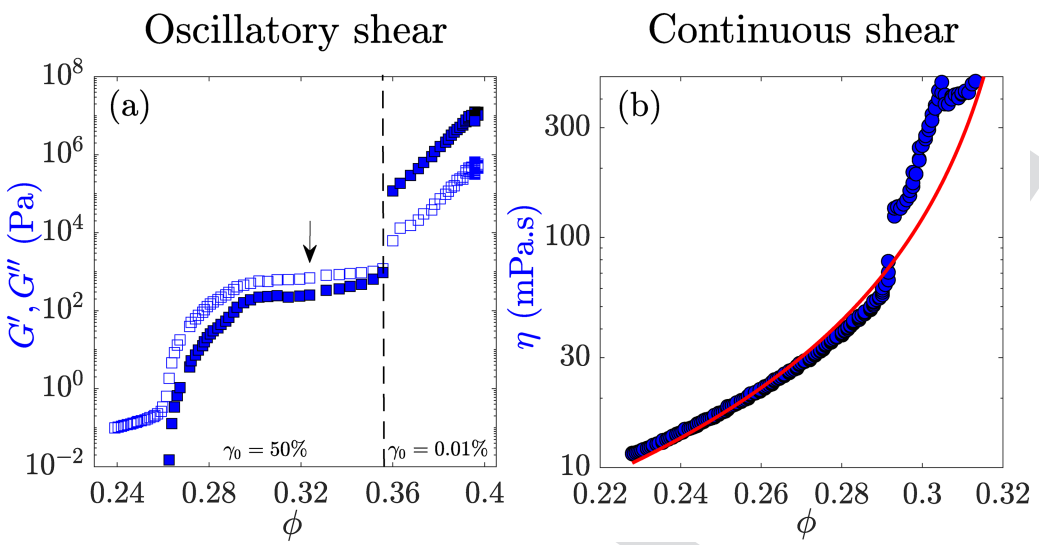

FIG. 7. Drying experiment on a suspension of silica nanoparticles of initial volume fraction $\phi_0 = 0.23$. Same data as in Figs. 6(d) and 6(h) reported as a function of the volume fraction ϕ inferred from the gap decrease [Figs. 6(b) and 6(f), respectively]. (a) G' (■) and G'' (□) vs ϕ. The vertical dashed line highlights the volume fraction at which the strain amplitude is switched from $\gamma_0 = 50\%$ to $\gamma_0 = 0.01\%$. The black arrow highlights the critical $\phi_c^{(\mathrm{ref})} = 0.32$ beyond which a yield stress is expected [30]. (b) Shear viscosity $\eta = \sigma/\dot{\gamma}$ vs ϕ. The red curve corresponds to the Quemada model [see Eq. (4) in the text] with $\phi_c = 0.33$. Experiments performed at constant temperature ($T \simeq 21\,^\circ$C) in a parallel-plate geometry, with a transparent bottom plate.

where η_s is the viscosity of the solvent and $\phi_{\max}$ is the volume fraction at maximum packing. Such a model has been successfully applied to describe the rheology of Ludox suspensions [30,45]. Here too, this phenomenological model describes our data very well with $\phi_{\max} = 0.33$, in good agreement with the value expected for suspensions of Ludox HS-40. The fact that $\phi_{\max} < \phi_c$, and the good agreement of $\phi_{\max}$ with the literature, confirms that the sample remains more spatially homogeneous during the experiment performed under continuous shear. Indeed, assuming a linear gradient of concentration following the steps discussed in Sec. III B yields negligible values of α [see Fig. 10(b) in Appendix C]. This result shows that drying experiments performed under continuous shear yield more accurate values of ϕ_c than experiments performed under oscillatory shear.

IV. CONCLUSION

The ZNF protocol has been successfully applied to perform time-resolved rheological measurements during the drying of Newtonian fluids and colloidal suspensions. This protocol can be employed with both oscillatory shear and continuous shear to measure in a single experiment with only one sample loading what is usually obtained with multiple measurements on samples of various concentrations, in the absence of evaporation. Moreover, we have shown that in comparison to oscillatory shear experiments, continuous shear at moderate intensity allows for the homogenization of the sample, which limits the growth of spatial gradients and, therefore, leads to more accurate rheological measurements. This work constitutes a proof of concept and opens new perspectives for determining the macroscopic rheological properties of viscoelastic samples subject to solvent evaporation and monitor their eventual solgel or glass transition. Moreover, we have observed that depending on the shear intensity applied during the dehydration of the sample, one may control the spatial gradient of concentration that builds up in a sample, which is sandwiched between two parallel disks and dries along the radial direction. As such, beyond providing an accurate method for bulk rheological measurements on drying samples, our work suggests a simple way of making solids with spatially modulated mechanical properties. Future work will be focused on the characterization of the local mechanical properties of such heterogeneous solids produced from the drying of colloidal suspensions under external shear.

ACKNOWLEDGMENTS

The authors thank M. Lenz, S. Manneville, B. Mao, G. H. McKinley, and J.-B. Salmon for fruitful discussions and acknowledge the support from the Fonds ESPCI Paris and the MIT-France program from the MIT International Science and Technology Initiative.

APPENDIX A: LONG-DURATION DRYING EXPERIMENT ON WATER

To complement the drying experiments performed on distilled water over a short duration of typically 30 min, we report here the case of a 10 h-long experiment. The results, displayed in Fig. 8, show that the ZNF protocol allows us to measure accurately the viscosity of water, while the volume of the sample decreases by 60%.

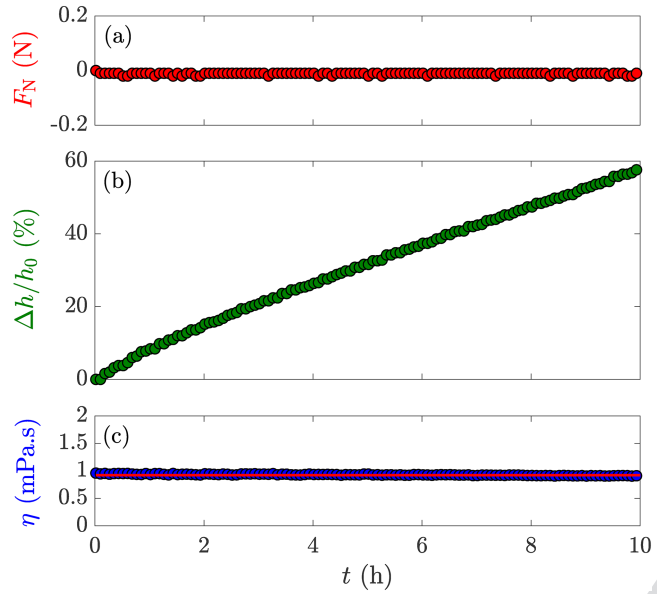

FIG. 8. Viscosity measurement under continuous shear ($\dot{\gamma}$ =10 s^{-1}) on a drying water sample using the ZNF protocol over 10 h. Temporal evolution of (a) the applied normal force F_N, (b) the relative gap decrease $\Delta h/h_0$, and (c) the shear viscosity $\eta = \sigma/\dot{\gamma}$. Experiments performed at $T = 25\,^{\circ}$C, with $h_0 = 500\,\mu$m. In (c), the red line corresponds to the mean value of the viscosity computed over the whole duration of the experiment $\eta = (0.92 \pm 0.02)$ mPa s.

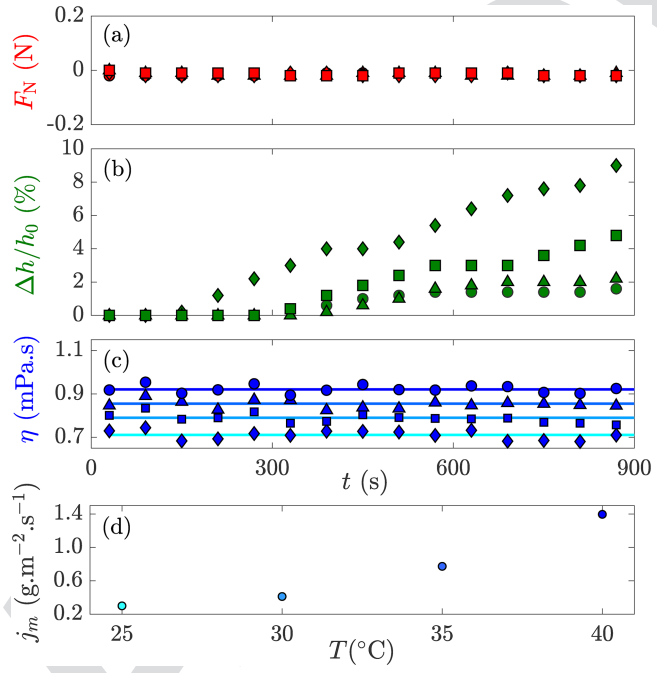

FIG. 9. Viscosity measurement with the ZNF protocol under continuous shear ($\dot{\gamma} = 10\,$s^{-1}) on a drying water sample at different temperatures. Temporal evolution of (a) the applied normal force F_N, (b) the relative gap decrease $\Delta h/h_0$, and (c) the shear viscosity $\eta = \sigma/\dot{\gamma}$. Experiments performed at $T = 25\,^{\circ}$C (△), 30 °C (○), 35 °C (□), and 40 °C (◇), with $h_0 = 500\,\mu$m. In (c), the continuous lines correspond to the mean value of the viscosity computed over the duration of the experiment, i.e., $\eta = (0.92 \pm 0.01)$ mPa s, $\eta = (0.85 \pm 0.02)$ mPa s, $\eta = (0.78 \pm 0.02)$ mPa s, and $\eta = (0.71 \pm 0.02)$ mPa s for increasing temperatures. (d) Mass fluxes of water leaving the shear cell due to evaporation vs temperature.

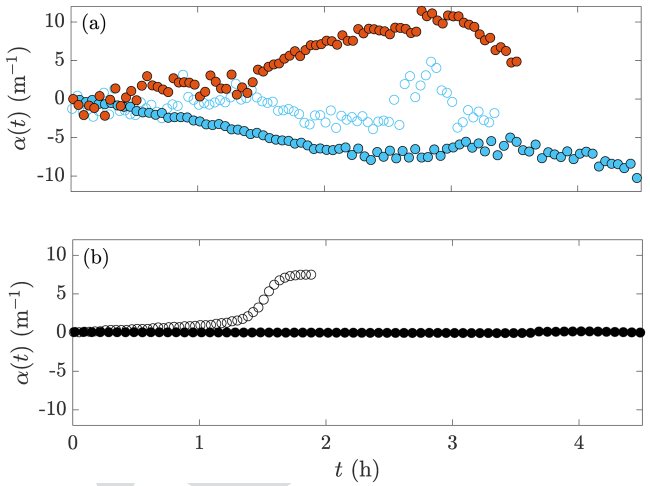

FIG. 10. Temporal evolution of slopes of the linear gradients α for (a) a water–glycerol mixture with an initial mass fraction of 20 wt. % under oscillatory shear [$f_0 = 0.5$ Hz, $\gamma_0 = 50\%$: (•)] and continuous shear [$\dot{\gamma} = 10\,$s^{-1} : (○), $\dot{\gamma} = 100\,$s^{-1} : (•)], and for (b) a suspension of silica nanoparticles of initial volume fraction $\phi_0 = 0.23$ under oscillatory shear before the crossing of G' and G'' [$f_0 = 1$ Hz, $\gamma_0 = 50\%$: (○)] and continuous shear [$\dot{\gamma} = 10\,$s^{-1}: (•)].

APPENDIX B: IMPACT OF TEMPERATURE ON THE DRYING RATE

Here, we show in Fig. 9 that the ZNF protocol allows us to monitor accurately the viscosity of distilled water drying at different temperatures, ranging between 25 and 40 °C.

APPENDIX C: ESTIMATE OF THE LINEAR GRADIENT

We report in Fig. 10 the values of the computed linear gradients α for the experiments performed on water–glycerol mixtures [Fig. 10(a)] and suspensions of silica colloids [Fig. 10(b)]. We show that the concentration gradients due to the solvent evaporation are positive under oscillatory shear and continuous shear of moderate intensity ($\dot{\gamma} = 10\,$s^{-1}), whereas the gradient is negative under the continuous shear of larger intensity ($\dot{\gamma} = 100\,$s^{-1}). We do not observe any gradient for a drying experiment performed on a suspension of silica particles under continuous shear ($\dot{\gamma} = 100\,$s^{-1}).

APPENDIX D: DRYING WATER–GLYCEROL MIXTURE UNDER LARGE CONTINUOUS SHEAR

We show in Fig. 11 the viscosity measurement of a water–glycerol mixture (initial content of 20 wt. % in glycerol) under continuous shear ($\dot{\gamma} = 100\,$s^{-1}). Contrary to the case of $\dot{\gamma} = 10\,$s^{-1} that is reported in the main text in Figs. 4(e)–4(h), one can see the formation of a positive gradient of concentration, i.e., water accumulates at the periphery of the shear cell beyond $t = 1$ h [Fig. 11(d)]. Concomitantly, the data reported in Fig. 11(c) clearly show the departure of the measured viscosity from the expected value for spatially homogeneous drying.

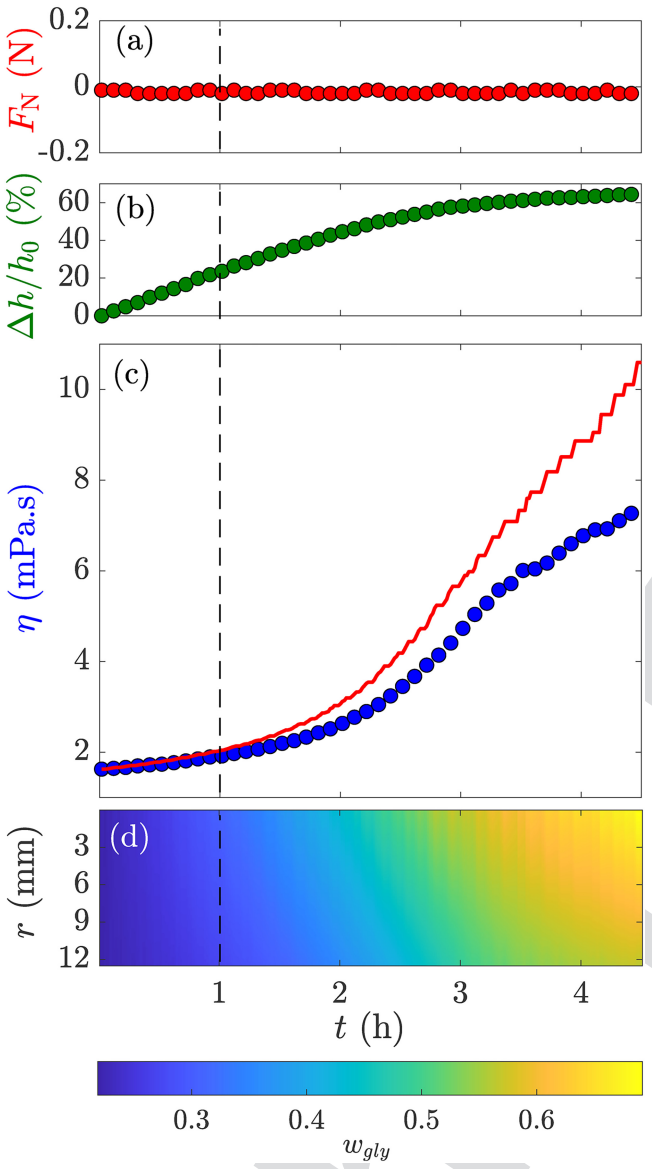

FIG. 11. Viscosity measurement with the ZNF protocol under continuous shear ($\dot{\gamma} = 100\,\mathrm{s}^{-1}$) on a drying water–glycerol mixture, with an initial glycerol content of 20 wt. %. Temporal evolution of (a) the applied normal force F_N, (b) the relative gap decrease $\Delta h/h_0$, (c) the shear viscosity $\eta = \sigma/\dot{\gamma}$, and (d) the computed temporal evolution of a linear gradient in the sample. The experiment is performed at $T = 25\,^\circ\mathrm{C}$. The continuous red curve corresponds to the tabulated values [36] of the shear viscosity of water–glycerol mixtures at $T = 25\,^\circ\mathrm{C}$, assuming that the glycerol concentration, inferred from the gap decrease, remains homogeneous at all time. The vertical dashed line corresponds to the time beyond which the glycerol concentration is not homogeneous along the radial direction.

REFERENCES

[1] Boger, D. V., and A. V. Rama Murthy, "Note: Normal stress measurement and evaporation effects on the Weissenberg rheogoniometer," Trans. Soc. Rheol. **13**, 405–408 (1969).

[2] Macosko, C., *Rheology: Principles, Measurements, and Applications* (Wiley-VCH, New York, 1994).

[3] Ewoldt, R. H., M. T. Johnston, and L. M. Caretta, "Experimental challenges of shear rheology: How to avoid bad data," in *Complex Fluids in Biological Systems* (Springer, Berlin, 2015), pp. 207–241.

[4] Orafidiya, L. O., "Continuous shear rheometry of o/w emulsions; control of evaporation in cone/plate geometry," J. Pharm. Pharmacol. **41**, 341–342 (1989).

[5] Wee, W.-K., and M. Mackley, "The rheology and processing of a concentrated cellulose acetate solution," Chem. Eng. Sci. **53**, 1131–1144 (1998).

[6] Sato, J., and V. Breedveld, "Evaporation blocker for cone-plate rheometry of volatile samples," Appl. Rheol. **15**, 390–397 (2005).

[7] Lee, C. H., Y. Lu, and A. Q. Shen, "Evaporation induced self assembly and rheology change during sol-gel coating," Phys. Fluids **18**, 052105 (2006).

[8] Prevo, B. G., D. M. Kuncicky, and O. D. Velev, "Engineered deposition of coatings from nano- and micro-particles: A brief review of convective assembly at high volume fraction," Colloids Surf., A **311**, 2–10 (2007), Engineering Particle Technology.

[9] Leng, J., B. Lonetti, P. Tabeling, M. Joanicot, and A. Ajdari, "Microevaporators for kinetic exploration of phase diagrams," Phys. Rev. Lett. **96**, 084503 (2006).

[10] Merlin, A., J.-B. Salmon, and J. Leng, "Microfluidic-assisted growth of colloidal crystals," Soft Matter **8**, 3526–3537 (2012).

[11] Lidon, P., and J.-B. Salmon, "Dynamics of unidirectional drying of colloidal dispersions," Soft Matter **10**, 4151–4161 (2014).

[12] Piroird, K., V. Lazarus, G. Gauthier, A. Lesaine, D. Bonamy, and C. L. Rountree, "Role of evaporation rate on the particle organization and crack patterns obtained by drying a colloidal layer," Europhys. Lett. **113**, 38002 (2016).

[13] Endruweit, A., M. S. Johnson, and A. C. Long, "Curing of composite components by ultraviolet radiation: A review," Polym. Compos. **27**, 119–128 (2006).

[14] Poth, U., "Drying oils and related products," in *Ullmann's Encyclopedia of Industrial Chemistry* (American Cancer Society, Atlanta, GA, 2001).

[15] Zhou, C., X. Lu, Z. Xin, J. Liu, and Y. Zhang, "Hydrophobic benzoxazine-cured epoxy coatings for corrosion protection," Prog. Org. Coat. **76**, 1178–1183 (2013).

[16] Fudge, D. S., T. Winegard, R. Ewoldt, D. Beriault, L. Szewciw, and G. McKinley, "From ultra-soft slime to hard α-keratins: The many lives of intermediate filaments," Integr. Comp. Biol. **49**, 32–39 (2009).

[17] Miserez, A., T. Schneberk, C. Sun, F. W. Zok, and J. H. Waite, "Dynamic light scattering at low rates of shear," Science **319**, 1816–1819 (2008).

[18] Zakharov, P., and F. Scheffold, "Monitoring spatially heterogeneous dynamics in a drying colloidal thin film," Soft Mater. **8**, 102–113 (2010).

[19] Molenaar, F., T. Svanholm, and A. Toussaint, "Rheological behaviour of latexes in-can and during film drying," Prog. Org. Coat. **30**, 141–158 (1997).

[20] Figliuzzi, B., D. Jeulin, A. Lemaître, G. Fricout, J. J. Piezanowski, and P. Manneville, "Rheology of thin films from flow observations," Exp. Fluids **53**, 1289–1299 (2012).

[21] Bodiguel, H., and J. Leng, "Imaging the drying of a colloidal suspension," Soft Matter **6**, 5451–5460 (2010).

[22] Kim, J. C., M. Seo, M. A. Hillmyer, and L. F. Francis, "Magnetic microrheology of block copolymer solutions," ACS Appl. Mater. Interfaces **5**, 11877–11883 (2013).

[23] Komoda, Y., L. G. Leal, and T. M. Suires, "Local, real-time measurement of drying films of aqueous polymer solutions using active microrheology," Langmuir **30**, 5230–5237 (2014).

[24] Castro, D. J., J.-O. Song, R. K. Lade, and L. F. Francis, "Magnetic microrheology for characterization of viscosity in coatings," in *Protective Coatings: Film Formation and Properties*, edited by M. Wen and K. Dušek (Springer, Cham, 2017), pp. 115–136.

[25] Mao, B., T. Divoux, and P. Snabre, "Normal force controlled rheology applied to agar gelation," J. Rheol. **60**, 473–489 (2016).

[26] Mao, B., A. Bentaleb, F. Louerat, T. Divoux, and P. Snabre, "Heat-induced aging of agar solutions: Impact on the structural and mechanical properties of agar gels," Food Hydrocolloids **64**, 59–69 (2017).

[27] Beniazza, R., N. Bayo, D. Jardel, R. Rust, B. Mao, T. Divoux, M. Schmutz, F. Castet, G. Raffy, A. Del Guerzo, N. D. McClenaghan, T. Buffeteau, and J.-M. Vincent, "A fluorous sodium l-prolinate derivative as low molecular weight gelator for perfluorocarbons," Chem Commun. **56**, 8655–8658 (2020).

[28] Mao, B., A. Bouchaudy, J.-B. Salmon, T. Divoux, and P. Snabre, "Time-resolved rheological monitoring of viscoelastic materials under drying," in *11*th *Annual European Rheology Conference, Copenhagen, Denmark* (KU Leuven, Leuven, 2017).

[29] Loussert, C., A. Bouchaudy, and J.-B. Salmon, "Drying dynamics of a charged colloidal dispersion in a confined drop," Phys. Rev. Fluids **1**, 084201 (2016).

[30] Di Giuseppe, E., A. Davaille, E. Mittelstaedt, and M. François, "Rheological and mechanical properties of silica colloids: From newtonian liquid to brittle behaviour," Rheol. Acta **51**, 451–465 (2012).

[31] Boulogne, F., L. Pauchard, F. Giorgiutti-Dauphiné, R. Botet, R. Schweins, M. Sztucki, J. Li, B. Cabane, and L. Goehring, "Structural anisotropy of directionally dried colloids," Europhys. Lett. **105**, 38005 (2014).

[32] Ziane, N., and J.-B. Salmon, "Solidification of a charged colloidal dispersion investigated using microfluidic pervaporation," Langmuir **31**, 7943–7952 (2015).

[33] Gatapova, E. Y., A. A. Semenov, D. V. Zaitsev, and O. A. Kabov, "Evaporation of a sessile water drop on a heated surface with controlled wettability," Colloids Surf. Physicochem. Eng. Asp. **441**, 776–785 (2014).

[34] Kuznetsov, G., S. Kralinova, I. Voytkov, and A. Islamova, "Rates of high-temperature evaporation of promising fire-extinguishing liquid droplets," Appl. Sci. **9**, 5190 (2019).

[35] Sobac, B., and D. Brutin, "Thermal effects of the substrate on water droplet evaporation," Phys. Rev. E **86**, 021602 (2012).

[36] Cheng, N.-S., "Formula for the viscosity of a glycerol-water mixture," Ind. Eng. Chem. Res. **47**, 3285–3288 (2008).

[37] Daubersies, L., and J.-B. Salmon, "Evaporation of solutions and colloidal dispersions in confined droplets," Phys. Rev. E **84**, 031406 (2011).

[38] Nakagawa, H., and T. Oyama, "Molecular basis of water activity in glycerol–water mixtures," Front. Chem. **7**, 731 (2019).

[39] D'Errico, G., O. Ortona, F. Capuano, and V. Vitagliano, "Diffusion coefficients for the binary system glycerol + water at 25 °C, A velocity correlation study," J. Chem. Eng. Data **49**, 1665–1670 (2004).

[40] Montgomery, T. S., and Z. L. Zhizhong, "Single-point determination of nonlinear rheological data from parallel-plate torsional flow," Appl. Rheol. **16**, 70–79 (2006).

[41] Rusu, D., D. Genoe, P. van Puyvelde, E. Peuvrel-Disdier, P. Navard, and G. Fuller, "Dynamic light scattering during shear: Measurements of diffusion coefficients," Polymer **40**, 1353–1357 (1999).

[42] Cipelletti, L., H. Bissig, V. Trappe, P. Ballesta, and S. Mazoyer, "Time-resolved correlation: A new tool for studying temporally heterogeneous dynamics," J. Condens. Matter Phys. **15**, S257–S262 (2002).

[43] Divoux, T., B. Mao, and P. Snabre, "Syneresis and delayed detachment in agar plates," Soft Matter **11**, 3677–3685 (2015).

[44] Quemada, D., "Rheology of concentrated disperse systems and minimum energy dissipation principle," Rheol. Acta **16**, 82–94 (1977).

[45] Sobac, B., S. Dehaeck, A. Bouchaudy, and J.-B. Salmon, "Collective diffusion coefficient of a charged colloidal dispersion: Interferometric measurements in a drying drop," Soft Matter **16**, 8213–8225 (2020).